The dynamic characteristics of harvesting energy from mechanical vibration via piezoelectric conversion*

Fan Kang-Qi(樊康旗)†, Ming Zheng-Feng(明正峰), Xu Chun-Hui(徐春辉), and Chao Feng-Bo(晁锋波)

School of Electronical & Mechanical Engineering, Xidian University, Xi'an 710071, *China*

(Received 18 December 2012; revised manuscript received 1 April 2013)

As an alternative power solution for low-power devices, harvesting energy from the ambient mechanical vibration has received increasing research interest in recent years. In this paper we study the transient dynamic characteristics of a piezoelectric energy harvesting system including a piezoelectric energy harvester, a bridge rectifier, and a storage capacitor. To accomplish this, this energy harvesting system is modeled, and the charging process of the storage capacitor is investigated by employing the in-phase assumption. The results indicate that the charging voltage across the storage capacitor and the gathered power increase gradually as the charging process proceeds, whereas the charging rate slows down over time as the charging voltage approaches to the peak value of the piezoelectric voltage across the piezoelectric materials. In addition, due to the added electrical damping and the change of the system natural frequency when the charging process is initiated, a sudden drop in the vibration amplitude is observed, which in turn affects the charging rate. However, the vibration amplitude begins to increase as the charging process continues, which is caused by the decrease in the electrical damping (i.e., the decrease in the energy removed from the mechanical vibration). This electromechanical coupling characteristic is also revealed by the variation of the vibration amplitude with the charging voltage.

Keywords: piezoelectric conversion, mechanical vibration, charging dynamics, electromechanical coupling

PACS: 45.20.dg, 46.70.De, 68.35.Gy **DOI:** 10.1088/1674-1056/22/10/104502

1. Introduction

Low-power devices (such as wireless sensors and transmitters, medical implant sensors, portable electronic devices) and the relevant physical mechanisms have been the subject of a great deal of research over the past few years.[1–5] Potential applications of these low-power devices include building and machinery status monitoring,[6] natural disaster relief,[7] hazardous environment exploration,[1] biomedical health monitoring,[2] and military target tracking and surveillance.[8] However, as low-power devices increase in number and decrease in size, the proliferation of these devices raises the problem of an effective power supply. The conventional solution is to use electrochemical batteries for power. The limitation of battery power is that it needs frequent replacement/recharging, which is costly and cumbersome for a large quantity or in a remote area.

To tackle this issue, many research efforts have been devoted to harvesting energy from the ambient environment to power and maintain these low-power devices.[9–13] Such energy transducers are termed microenergy harvesters or micropower generators.[14–16] Currently, the harvestable environmental sources mainly include solar power, thermal gradients, and mechanical vibration. Among them, mechanical vibration is ubiquitous, and is easily converted into electricity through micro-electro-mechanical systems (MEMS) technology.[17] The most widely used mechanism for converting mechanical vibration into electricity is piezoelectric conversion because it has the advantages of low mechanical damping, strong electromechanical coupling, appropriate voltage and current output, and compatibility with MEMS processes.[17,18]

A vibrating piezoelectric element in a piezoelectric energy harvester (PEH) generates an alternating current (AC), while the low-power devices generally require a stabilized direct current (DC). Therefore, an interface circuit is usually demanded in practical applications to ensure the electrical compatibility between a PEH and a low-power device. The standard interface circuit involves only a bridge rectifier for AC–DC conversion.[19] Significant studies have been devoted to optimizing the interface circuit to maximize the power output of a PEH. For example, DC–DC converter circuits have been investigated to match the actual load of a low-power device to the impedance of a PEH, thus maximizing the power output.[20] Furthermore, a synchronous electric charge extraction method developed by Lefeuvre *et al.*[21] has been shown to increase the power output to 400% of the power output across a matched resistive load. In the subsequent studies, Lefeuvre *et al.*[22,23] proposed a new technique termed synchronous switch harvesting on inductor (SSHI), which has also been successful in increasing the PEH power output. Liu *et al.*[24] reported on an optimal work cycle for a PEH, and theoretically showed that their method yields more power than an SSHI. Hu *et al.*[25] developed a nonlinear interface circuit by

*Project supported by the National Natural Science Foundation of China (Grant No. 10476019) and the Fundamental Research Funds for the Central Universities (Grant No. K5051304011).

†Corresponding author. E-mail: kangqifan@gmail.com

© 2013 Chinese Physical Society and IOP Publishing Ltd

combining an SSHI and a DC–DC converter with a bridge rectifier, and found that their nonlinear interface circuit can raise the charging efficiency of a storage battery. Recently, an improved self-powered SSHI reported by Liang and Liao[19] has proved to harvest up to 200% more power than the standard interface circuit. In addition, the power dissipation resulting from the switch elements of an interface circuit was studied by Ming and Zhou.[26]

The research work cited above focused primarily on developing an optimal interface circuit to maximize the power output of a PEH. However, the energy harvested from the mechanical vibration is usually time-varying and insufficient to power the low-power devices directly. To account for this, most low-power devices adopt low duty cycle designs, meaning that most of the time the devices are idle and periodically turned on for very short intervals.[27] For a low duty cycle design, an energy storage buffer is indispensable for storing and accumulating the harvested energy. Rechargeable batteries and supercapacitors are two candidates for this energy storage purpose. A detailed study showed that supercapacitors are superior to rechargeable batteries in terms of charge–discharge efficiencies, energy density, adaptability, and lifetime.[28] Understanding the dynamic characteristics of charging a storage capacitor by a PEH is critical to developing a system that maximizes the duty cycle of a low-power device.[27,29] However, the most published papers generally only consider simple resistive loads,[30–33] or only focus on the frequency response characteristics of the output voltage and output power of a PEH.[34–37]

In the present paper, an electromechanical model is proposed to study the dynamic behaviors of an energy harvesting system. This system includes a PEH, a bridge rectifier, and a storage capacitor to accumulate the electrical energy converted from the ambient mechanical vibration. Without an external resistive load, the accumulation of the electrical energy in the storage capacitor is a time-varying transient process. To predict the dynamic characteristics related to this time-varying transient process, an analytical model concerning the electromechanical coupling between the energy storage and the mechanical vibration is derived based on the in-phase assumption. The comparison between this analytical model and related experimental data indicates that the analytical model could predict the energy harvesting and storage capacities of this type of energy harvesting system.

2. Energy harvesting system model

2.1. PEH model

A PEH reference configuration is composed of two piezoelectric layers and a metal shim, i.e., a triple-layer piezoelectric cantilever beam as shown in Fig. 1. This triple-layer piezoelectric cantilever beam is designed to operate in the transverse mode (3–1 mode), which is the general case for the bending deformation. When the mass block affixed at the free end of the piezoelectric cantilever beam is forced to vibrate by the ambient mechanical vibration, an applied mechanical stress T_1 along axis-1 is produced in the piezoelectric layer, which induces an electric displacement D_3 along axis-3. In the meantime, the applied electrical field E_3 along axis-3 affects the mechanical strain S_1 along axis-1. The coupling equations for 3–1 mode are

$$D_3 = d_{31}T_1 + \varepsilon_{33}E_3, \tag{1}$$

$$S_1 = s_{11}T_1 + d_{31}E_3, \tag{2}$$

where s_{11}, ε_{33}, and d_{31} are the compliance, permittivity, and piezoelectric coefficient of the piezoelectric material, respectively.

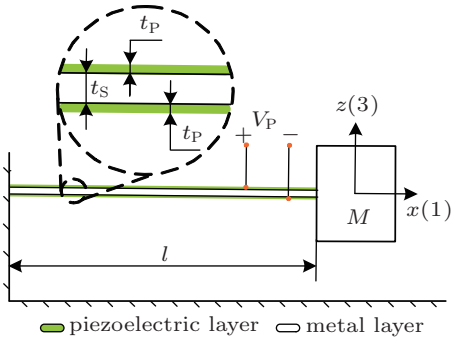


Fig. 1. (color online) Schematic diagram of a PEH.

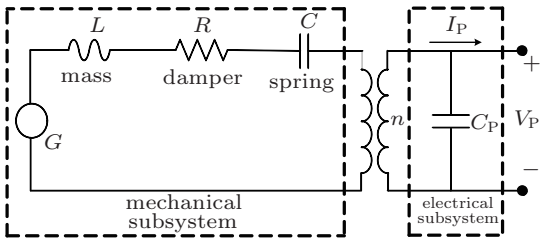


Fig. 2. Equivalent circuit model of the PEH.

The electromechanical behavior of the considered PEH can be represented by an equivalent circuit model in which each of the mechanical properties of the PEH is replaced by an equivalent electric component as shown in Fig. 2. For example, the equivalent inductor L represents the effective mass (M) of the PEH. Similarly, G (voltage generator), C (capacitor), and R (resistor) represent the stress (T), compliance (s), and damping (η) of the PEH, respectively. The transformer, representing the piezoelectric coupling, is characterized by a turn ratio (n) that relates the stress in the mechanical subsystem to the voltage in the electrical subsystem. The resulting dynamics of the PEH operating in 3–1 mode can thus be described by [34]

$$G = L\ddot{S}_1 + R\dot{S}_1 + \frac{S_1}{C} + nV_P, \tag{3}$$

$$I_P = C_P\dot{V}_P, \tag{4}$$

where C_P is the capacitance of the piezoelectric layers (intrinsic capacitor), V_P is the voltage across the piezoelectric layers (piezoelectric voltage), and I_P is the resulting current.

In order to study the effects of electromechanical coupling on the mechanical vibration of the piezoelectric cantilever beam, we need to return the equivalent circuit model of the mechanical subsystem to a vibration equation. Using the expressions for G, L, R, C, n, I_P, and S_1 (see Ref. [34] for detailed discussion), equations (3) and (4) can be rewritten respectively as

$$M\ddot{z}+\eta\dot{z}+Kz+\Theta_1 V_P = F(t), \tag{5}$$
$$\Theta_2\dot{z} = C_P\dot{V}_P, \tag{6}$$

where z is the displacement of the beam tip, K is the effective stiffness of the beam, $F(t)$ is the external excitation, Θ_1 and Θ_2 are the effective piezoelectric coefficients, representing force factor and current factor, respectively. K, Θ_1, and Θ_2 are determined respectively by

$$K = \frac{Y_P}{k_1 k_2},$$
$$\Theta_1 = \frac{\alpha d_{31} Y_P}{2t_P k_1},$$
$$\Theta_2 = \frac{\alpha w l d_{31} Y_P}{k_2},$$

where Y_P is the elastic constant of the piezoelectric material, α is equal to 1 or 2 for piezoelectric layers connected respectively in series or parallel, k_1 and k_2 are two constants related to material properties and structural geometry,[34] w and l are beam width and length, respectively.

The effective piezoelectric coefficient Θ_1, also called backward electromechanical coupling coefficient, describes the effect of the generated piezoelectric voltage on the mechanical vibration of a PEH by the term $\Theta_1 V_P$ in Eq. (5). In the meanwhile, the forward electromechanical coupling coefficient Θ_2 depicts the relationship between the generated current and the mechanical vibration of a PEH by the term $\Theta_2\dot{z}$ in Eq. (6). Moreover, Θ_1 and Θ_2 depend not only on the material properties and structural geometry of a PEH, but also on the connection mode of the two piezoelectric layers. In some previous studies, Θ_1 was chosen to be equal to Θ_2.[17,27,29] However, different modeling methods or load conditions could lead to the case that Θ_1 is different from Θ_2 (including the case that Θ_1 is assumed to be zero)[36,38,39] as shown by Eqs. (5) and (6). Therefore the PEH model proposed here could be considered as a generalized version of the model in which Θ_1 is equal to Θ_2.

2.2. Energy harvesting system model

The energy harvesting system includes a PEH, a bridge rectifier, and a storage capacitor as illustrated in Fig. 3. The AC electrical energy generated by the vibrating piezoelectric cantilever beam (i.e., PEH) is converted into DC electrical energy by a standard interface circuit (bridge rectifier), and then is stored in a supercapacitor. The governing equations of this energy harvesting system can be described by

$$M\ddot{z}+\eta\dot{z}+Kz+\Theta_1 V_P = F(t), \tag{7}$$
$$-\Theta_2\dot{z}+C_P\dot{V}_P = -I, \tag{8}$$

where I is the rectified output current, and $F(t)$ is the external mechanical excitation. Note that in most vibration-based energy harvesting systems, $F(t)$ originates from the mechanical vibration of the base.

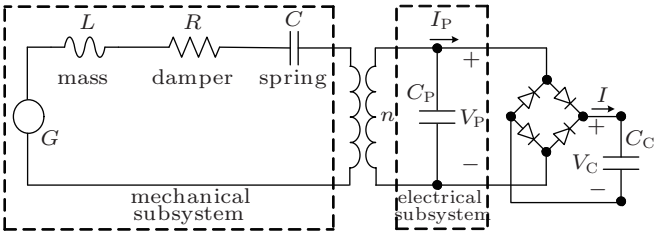


Fig. 3. Schematic diagram of the energy harvesting system.

During the charging process, the charging voltage (i.e., the voltage across the storage capacitor) increases continuously, whereas the piezoelectric voltage generated by the PEH vibrates periodically as shown in Fig. 4. In the i-th half cycle defined by $i\pi \le \omega t \le (i+1)\pi$ and shown in Fig. 5, the piezoelectric voltage $V_P(t)$ is smaller in magnitude than the charging voltage $V_C(t)$ from $i\pi$ to P_i, and thus the rectifying bridge is blocked. At the phase P_i, the magnitude of $V_P(t)$ reaches that of $V_C(t)$, and then the rectifying bridge begins to conduct and the magnitudes of $V_P(t)$ and of $V_C(t)$ increase simultaneously due to the continuous bending of the beam. At the end of the i-th half cycle, the rectifying bridge is blocked again since the beam deflection and the generated piezoelectric voltage begin to decrease. Thus, the output current charging the storage capacitor is

$$I(t) = \begin{cases} 0, & \text{for } i\pi \le \omega t \le P_i, \\ \left|C_C\dot{V}_C(t)\right|, & \text{for } P_i \le \omega t \le (i+1)\pi. \end{cases} \tag{9}$$

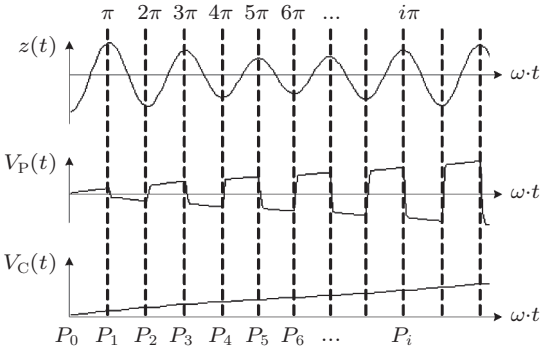


Fig. 4. Schematic diagram of the charging process.

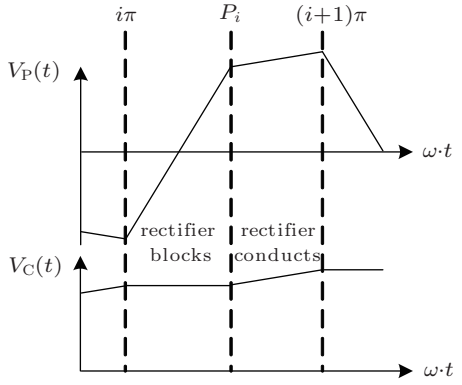


Fig. 5. The i-th half cycle of the charging process.

The energy harvesting system model described by Eqs. (7) and (8) captures the electromechanical coupling characteristics of the piezoelectric energy harvesting system. For example, equation (7) describes the effect of the generated piezoelectric voltage on the mechanical vibration by the term $\Theta_1 V_{\rm P}$, whereas equation (8) depicts the conversion of mechanical vibration to a current source via current factor Θ_2. When the electromechanical coupling is strong, which is the case considered in this study, the in-phase assumption has proved to be accurate at identifying the electromechanical coupling characteristics of the piezoelectric energy harvesting system.[29,40] The in-phase assumption will be elaborated in the following subsection.

2.3. In-phase analysis of the energy harvesting system

2.3.1. In-phase assumption

In-phase assumption supposes that the applied excitation $F(t)$ is in phase with the vibration velocity $\dot{z}(t)$ of the piezoelectric cantilever beam. Precisely, the in-phase assumption is described by[17,40]

$$F(t) = \widehat{F}\sin(\omega t), \tag{10}$$

$$\dot{z}(t) = \widehat{z}\,\omega\sin(\omega t), \tag{11}$$

where $\widehat{z}$ is the vibration amplitude of the piezoelectric cantilever beam, $\widehat{F}$ and ω are the magnitude and angular frequency of the applied excitation, respectively.

Using the in-phase assumption, the coupling term $\Theta_2\dot{z}$ in Eq. (8) can be modeled as a current source $I_{\rm P}$, i.e.,

$$I_{\rm P}(t) = \Theta_2\dot{z}(t) = \Theta_2\widehat{z}\,\omega\sin(\omega t) = \widehat{I}_{\rm P}\sin(\omega t). \tag{12}$$

Then the output current charging the storage capacitor can be determined by

$$I(t) = \begin{cases} 0, & \text{for } i\pi \le \omega t \le P_i, \\ \dfrac{C_{\rm C}}{C_{\rm C}+C_{\rm P}}\left|\widehat{I}_{{\rm P},i}\sin(\omega t)\right|, & \text{for } P_i \le \omega t \le (i+1)\pi. \end{cases} \tag{13}$$

Here the subscript i is used in the term $\widehat{I}_{{\rm P},i}$ to show that the current flowing into the storage capacitor varies with each half cycle.

2.3.2. Charging voltage

The charging voltage increases as the charging process proceeds. In order to obtain the ever-increasing charging voltage in the i-th half cycle, integrating Eq. (8) over the interval $i\pi \le \omega t \le P_i$ yields[29]

$$\begin{aligned} &-\Theta_2\int_{i\pi/\omega}^{P_i/\omega}\dot{z}(t)\,{\rm d}t + C_{\rm P}\int_{i\pi/\omega}^{P_i/\omega}\dot{V}_{\rm P}(t)\,{\rm d}t \\ &= -\int_{i\pi/\omega}^{P_i/\omega}\widehat{I}_{{\rm P},i}\sin(\omega t)\,{\rm d}t + C_{\rm P}\left[V_{\rm P}(\omega t = P_i) - V_{\rm P}(\omega t = i\pi)\right] \\ &= \frac{\widehat{I}_{{\rm P},i}}{\omega}\left[\cos(P_i) - \cos(i\pi)\right] + C_{\rm P}\left[V_{\rm P}(P_i) - V_{\rm P}(i\pi)\right] \\ &= 0. \end{aligned} \tag{14}$$

If the storage capacitor is initially discharged, then $V_{\rm P}(P_i) = -V_{{\rm C},i}$ and $V_{\rm P}(i\pi) = V_{{\rm C},i}$ during the odd half cycles, whereas $V_{\rm P}(P_i) = V_{{\rm C},i}$ and $V_{\rm P}(i\pi) = -V_{{\rm C},i}$ during the even half cycles, where $V_{{\rm C},i}$ is the charging voltage at the end of the i-th half cycle as shown in Fig. 5. According to the foregoing discussion and Eq. (14), the critical point that the bridge rectifier initiates conducting in the i-th half cycle can be determined by

$$\cos(P_i) = \begin{cases} -1 + \dfrac{2\omega C_{\rm P}V_{{\rm C},i}}{\widehat{I}_{{\rm P},i}}, & i = 1,3,5,\ldots, \\ 1 - \dfrac{2\omega C_{\rm P}V_{{\rm C},i}}{\widehat{I}_{{\rm P},i}}, & i = 0,2,4,\ldots. \end{cases} \tag{15}$$

From the critical point P_i to $(i+1)\pi$, the bridge rectifier conducts, and the current flowing into the storage capacitor can be calculated by

$$\begin{aligned} \int_{{\rm P_i}/\omega}^{(i+1)\pi/\omega} I(t)\,{\rm d}t &= C_{\rm C}\int_{{\rm P_i}/\omega}^{(i+1)\pi/\omega}\dot{V}_{\rm C}(t)\,{\rm d}t \\ &= C_{\rm C}\left[V_{{\rm C},i+1} - V_{{\rm C},i}\right]. \end{aligned} \tag{16}$$

Substituting Eq. (13) into Eq. (16) yields

$$V_{{\rm C},i+1} = \begin{cases} V_{{\rm C},i} + \dfrac{\widehat{I}_{{\rm P},i}}{\omega}\dfrac{1}{C_{\rm P}+C_{\rm C}}\left[1-\cos(P_i)\right], & i = 1,3,5,\ldots, \\ V_{{\rm C},i} + \dfrac{\widehat{I}_{{\rm P},i}}{\omega}\dfrac{1}{C_{\rm P}+C_{\rm C}}\left[1+\cos(P_i)\right], & i = 0,2,4,\ldots. \end{cases} \tag{17}$$

Then by combining Eqs. (15) and (17), we can obtain the charging voltage by

$$\begin{aligned} V_{{\rm C},i+1} &= \frac{C_{\rm C}-C_{\rm P}}{C_{\rm C}+C_{\rm P}}V_{{\rm C},i} + \frac{2}{\omega\left(C_{\rm C}+C_{\rm P}\right)}\widehat{I}_{{\rm P},i} \\ &= \frac{C_{\rm C}-C_{\rm P}}{C_{\rm C}+C_{\rm P}}V_{{\rm C},i} + \frac{2\Theta_2}{C_{\rm C}+C_{\rm P}}\widehat{z}_i. \end{aligned} \tag{18}$$

2.3.3. Average power harvested during each half cycle

The average power harvested and stored in the storage capacitor during the i-th half cycle can be determined by

$$\begin{aligned}\bar{P}_i &= \frac{C_{\rm C}\left(V_{{\rm C},i+1}^2 - V_{{\rm C},i}^2\right)/2}{T/2} \\ &= \frac{\omega C_{\rm C}}{2\pi}\left\{\left[\left(\frac{C_{\rm C}-C_{\rm P}}{C_{\rm C}+C_{\rm P}}\right)^2 - 1\right]V_{{\rm C},i}^2 + \frac{4\Theta_2\left(C_{\rm C}-C_{\rm P}\right)}{\left(C_{\rm C}+C_{\rm P}\right)^2}V_{{\rm C},i}\widehat{z}_i \right. \\ &\quad \left. + \frac{4\Theta_2^2}{\left(C_{\rm C}+C_{\rm P}\right)^2}\widehat{z}_i^2\right\}, \end{aligned} \tag{19}$$

where T is the vibration period of the piezoelectric cantilever beam. In order to store the harvested power as much as possible during each half cycle, it is fairly reasonable to assume that $C_{\rm C} \gg C_{\rm P}$. Thus, equation (19) can be simplified into

$$\bar{P}_i = \frac{2\omega\left(\Theta_2\widehat{z}_i + C_{\rm C}V_{{\rm C},i}\right)\left(\Theta_2\widehat{z}_i - C_{\rm P}V_{{\rm C},i}\right)}{\pi\left(C_{\rm C}+2C_{\rm P}\right)}. \tag{20}$$

The power accumulated in the storage capacitor can then be calculated by

$$P_{\rm C} = \sum_i \bar{P}_i. \tag{21}$$

2.3.4. Vibration amplitude of the piezoelectric cantilever beam

To determine the effects of energy conversion and storage on the mechanical vibration of the piezoelectric cantilever beam, let equation (7) be multiplied by $\dot{z}(t)$ and equation (8) be multiplied by $V_{\rm P}(t)$, and integration of the addition of these two equations during each half cycle gives the equation of the energy balance

$$\begin{aligned}&\int_{i\pi/\omega}^{(i+1)\pi/\omega} F(t)\dot{z}(t){\rm d}t \\ &= \int_{i\pi/\omega}^{(i+1)\pi/\omega} \eta\dot{z}^2(t){\rm d}t + \int_{i\pi/\omega}^{(i+1)\pi/\omega}\left(\Theta_1-\Theta_2\right)V_{\rm P}(t)\dot{z}(t){\rm d}t \\ &\quad + \frac{1}{2}C_{\rm P}\left[V_{\rm P}^2\left(\left(i+1\right)\pi/\omega\right) - V_{\rm P}^2\left(i\pi/\omega\right)\right] + \bar{P}_i\frac{T}{2}. \end{aligned} \tag{22}$$

Noting that $V_{\rm P}(t) = \pm V_{\rm C}(t)$ at the beginning and end of each half cycle, and using the in-phase assumption, equation (22) can be reduced to

$$\begin{aligned}&\int_{i\pi/\omega}^{(i+1)\pi/\omega} F(t)\dot{z}(t){\rm d}t \\ &= \int_{i\pi/\omega}^{(i+1)\pi/\omega} \eta\dot{z}^2(t){\rm d}t + \frac{\Theta_1-\Theta_2}{\Theta_2}\int_{i\pi/\omega}^{(i+1)\pi/\omega} V_{\rm P}(t)I_{\rm P}(t){\rm d}t \\ &\quad + \frac{1}{2}C_{\rm P}\left[V_{{\rm C},i+1}^2 - V_{{\rm C},i}^2\right] + \bar{P}_i\frac{T}{2}. \end{aligned} \tag{23}$$

For the energy harvesting system shown in Fig. 3, a portion of the input energy that sources from the external mechanical excitation $F(t)$ is dissipated by the structural damping, and the remainder of the input energy is stored in the intrinsic capacitor and the storage capacitor. Therefore, the energy stored in the two capacitors in the i-th half cycle can be obtained by

$$E_{{\rm S},i} = \int_{i\pi/\omega}^{(i+1)\pi/\omega} F(t)\dot{z}(t){\rm d}t - \int_{i\pi/\omega}^{(i+1)\pi/\omega}\eta\dot{z}(t)^2{\rm d}t. \tag{24}$$

In terms of circuit theory, the energy stored in the intrinsic capacitor and the storage capacitor in the i-th half cycle can also be determined by

$$\begin{aligned}E_{{\rm S},i} &= \int_{i\pi/\omega}^{P_i/\omega} V_{\rm P}(t)I_{\rm P}(t){\rm d}t \\ &\quad + \int_{{\rm P_i}/\omega}^{(i+1)\pi/\omega}\left[V_{\rm P}(t)\cdot C_{\rm P}\dot{V}_{\rm P}(t) + V_{\rm C}(t)\cdot C_{\rm C}\dot{V}_{\rm C}(t)\right]{\rm d}t. \end{aligned} \tag{25}$$

Using Eq. (8), and taking into consideration $V_{\rm C}(t) = \pm V_{\rm P}(t)$ during the interval $P_i \le \omega t \le (i+1)\pi$, equation (25) can be simplified into

$$E_{{\rm S},i} = \int_{i\pi/\omega}^{(i+1)\pi/\omega} V_{\rm P}(t)I_{\rm P}(t){\rm d}t. \tag{26}$$

According to Eqs. (24) and (26), equation (23) can be expressed as

$$\begin{aligned}&\frac{2\Theta_2-\Theta_1}{\Theta_2}\int_{i\pi/\omega}^{(i+1)\pi/\omega} F(t)\dot{z}(t){\rm d}t \\ &= \frac{2\Theta_2-\Theta_1}{\Theta_2}\int_{i\pi/\omega}^{(i+1)\pi/\omega}\eta\dot{z}^2(t){\rm d}t + \frac{1}{2}C_{\rm P}\left[V_{{\rm C},i+1}^2 - V_{{\rm C},i}^2\right] \\ &\quad + \bar{P}_i\frac{T}{2}. \end{aligned} \tag{27}$$

Substituting Eqs. (18) and (20) into Eq. (27), and solving for $\widehat{z}_i$, we have

$$\widehat{z}_i = \frac{A - \sqrt{A^2 - 16B\Theta_2 C_{\rm C}C_{\rm P}V_{{\rm C},i}^2}}{2B}, \tag{28}$$

where A and B are given respectively by

$$\begin{aligned}A &= \pi\widehat{F}\Theta_1\left(C_{\rm C}+C_{\rm P}\right) - 2\pi\widehat{F}\Theta_2\left(C_{\rm C}+C_{\rm P}\right) \\ &\quad + 4V_{{\rm C},i}\Theta_2^2\left(C_{\rm C}-C_{\rm P}\right), \\ B &= \pi\eta\omega\Theta_1\left(C_{\rm C}+C_{\rm P}\right) - 2\pi\eta\omega\Theta_2\left(C_{\rm C}+C_{\rm P}\right) - 4\Theta_2^3. \end{aligned}$$

If the force factor Θ_1 is chosen to be equal to the current factor Θ_2, the analytical model given by Eqs. (18), (20), and (28) reduces to the model represented by Wickenheiser *et al.*[29] In addition, the effective piezoelectric coefficient Θ_1 given by Wickenheiser *et al.*[29] was obtained by the experiment, which poses a challenge to the structural optimization of a PEH since the relationship between the effective piezoelectric coefficient and the structural parameters was not presented. In contrast, the effective piezoelectric coefficients Θ_1 and Θ_2 given in this paper are determined by the structural parameters and material properties, which can facilitate the design and optimization of a PEH.

Other topics such as the conversion efficiency[41] and optimization[33] of the piezoelectric energy harvesting system will be studied and elaborated in separate papers.

3. Results and discussion

The energy harvesting system, illustrated in Figs. 1 and 3, is used to demonstrate the dynamic characteristics of harvesting energy from mechanical vibration via piezoelectric conversion. The piezoelectric material is PSI-5A4E ceramic, and the metal shim is made of brass. The structural parameters are given in Table 1. The intrinsic capacitor and the storage capacitor are originally discharged, and the charging process is initiated at 1.38 s (in accordance with the experiments[29]) after an external sinusoidal excitation with amplitude 2.5 mN and frequency 371 rad/s has been applied to the system. Other detailed experimental parameters can be found in Ref. [29].

Table 1. Structural parameters of the energy harvesting system.[29]

Structure size/mm	α	η/(N·s/m)	M/g	C_P/nF	C_C/μF
28.575×3.175×0.190	2	0.0115	1.1	13.48	13.29

In practical applications, the attainable charging voltage level is crucial for reducing the conduction loss and the quiescent power dissipation of a load circuit.[42] For the structural parameters adopted in this study, the variation of charging voltage $V_C(t)$ with time t and half-cycle number i during the charging process is shown in Fig. 6. It is obvious that the charging voltage $V_C(t)$ increases as the charging process progresses. However, as the charging process continues, it takes more time for the piezoelectric voltage $V_P(t)$ to reach the present voltage level of the storage capacitor during each half cycle, i.e., $P_i \to (i+1)\pi$ as $i \to \infty$, as illustrated in Figs. 4 and 5. As a result, the net charge stored in the storage capacitor during each half cycle decreases, and consequently, the charging rate slows down over time. The charging process terminates when the storage capacitor is charged to the peak value of the piezoelectric voltage. In this situation, the current passing through the bridge rectifier is zero, and the piezoelectric cantilever beam vibrates in an open-circuit condition. This charging process has also been experimentally observed by Wickenheiser *et al.*[29] using the same structural parameters as those used in this simulation. It can be seen that the charging voltage calculated in this study is in reasonable agreement with that obtained by the experiment.

Another key performance parameter of the energy harvesting system is the charging rate at which the power in the storage capacitor is accumulated to a desired level. The charging rate determines the duty period of a low-power device. For example, a typical industrial transceiver consumes around 0.1 W, and thus the energy harvesting system designed in this study can afford the transceiver to run every 4 s as shown in Fig. 7. Although the accumulated power in the storage capacitor increases with time increasing, the harvested power during each half-cycle (i.e., charging rate) decreases as the charging process proceeds as shown in Fig. 8. However, the initial part of the curve shown in Fig. 8 indicates that the charging behavior is not so simple, especially at the beginning of the charging process. A further study on the charging process shows that the charging rate is dependent on a combination of two factors: charging voltage $V_{C,i}$ and vibration amplitude $\widehat{z}_i$ as described by Eq. (20). Therefore, the different developing trends of $V_{C,i}$ and $\widehat{z}_i$, and the strong coupling between $V_{C,i}$ and $\widehat{z}_i$ shown by Eqs. (18) and (28) complicate the charging behavior.

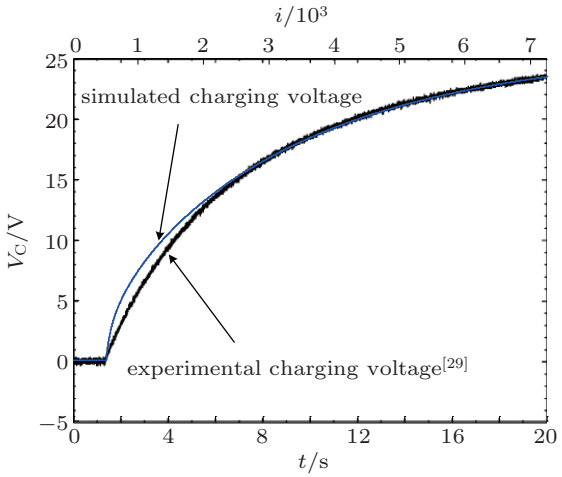


Fig. 6. (color online) Variation of charging voltage $V_C(t)$ with time t and half-cycle number i.

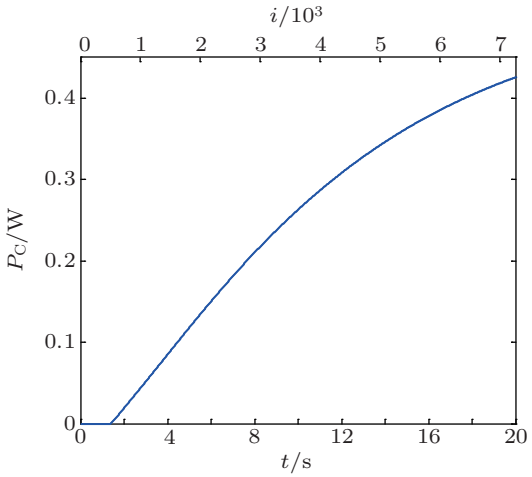


Fig. 7. (color online) Variation of accumulated power P_C with time t and half-cycle number i.

Piezoelectric energy harvesting systems are generally developed to convert mechanical energy into electrical energy, and thus they exhibit prominent electromechanical coupling characteristics. This can be revealed by the effect of electrical condition on the vibration amplitude of the piezoelectric cantilever beam as shown in Fig. 9. Initially, the bridge rectifier is blocked, and the piezoelectric cantilever beam vibrates in an open-circuit condition. Upon initiating the charging process, a sudden drop in the vibration amplitude can be

observed. As the charging process proceeds, the charging voltage approaches to the peak value of the piezoelectric voltage, and the decreasing energy is extracted from the vibration during each half cycle since it takes more time for the piezoelectric voltage to reach the present voltage level of the storage capacitor. This leads to decreased electrical damping and, consequently, increased vibration amplitude. Particularly, the piezoelectric cantilever beam returns to the initial open-circuit vibration status when the charging voltage reaches the peak value of the piezoelectric voltage. An experimental study conducted by Wickenheiser *et al.*[29] showed that the vibration amplitude of the piezoelectric cantilever beam could be reduced by over 40% after the piezoelectric layers had been connected to the interface circuit, and then the vibration amplitude increased as the charging process progresses as shown in Fig. 10. Wickenheiser *et al.*[29] argued that the sudden drop in the vibration amplitude was caused by the change in the system natural frequency when the energy harvesting system was changed from open-circuit condition to short-circuit condition. A further study on the harvested power $\bar{P}_i$ indicates that electrical damping could also reduce the variation amplitude significantly since $\bar{P}_i$ is pronounced even after 7000 half cycles as shown in Fig. 8.

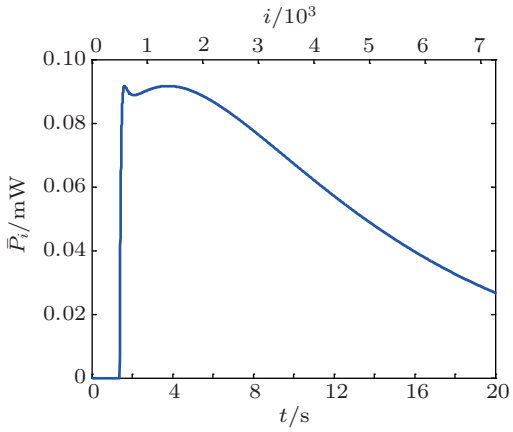


Fig. 8. (color online) Variation of harvested power $\bar{P}_i$ with time t and half-cycle number i.

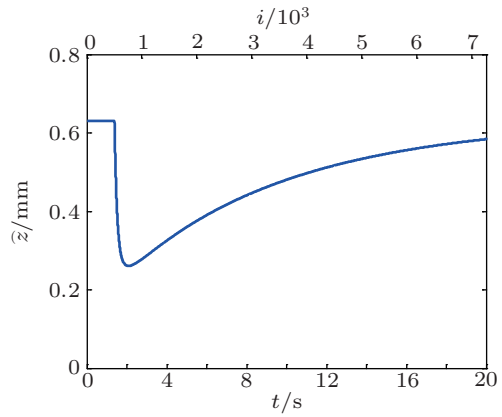


Fig. 9. (color online) Simulated variation of vibration amplitude $\widehat{z}$ with time t and half-cycle number i.

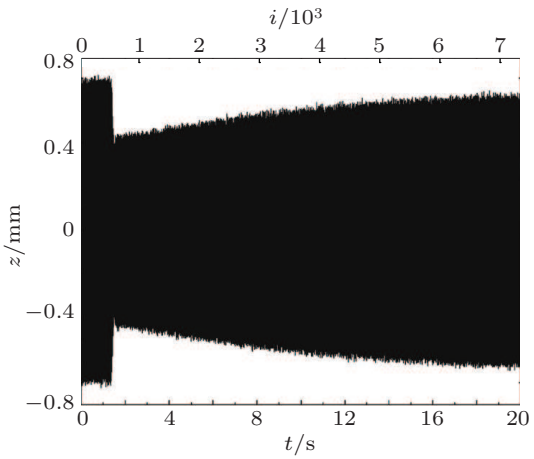


Fig. 10. Vibration of the piezoelectric cantilever beam obtained by experiment.[29]

The electromechanical coupling characteristics of this energy harvesting system can also be revealed by the variation of the vibration amplitude with the charging voltage as shown in Fig. 11. Due to the added electrical damping and the change in the system natural frequency, the vibration amplitude decreases as the charging voltage increases from 0 V to 5.6 V. As the charging process proceeds, the energy removed from the vibration during each half cycle decreases, resulting in reduced electrical damping. In addition, the frequency change is only significant at the beginning of the charging process and decays over time.[29] Therefore, the vibration amplitude increases gradually after the storage capacitor has been charged to 5.6 V.

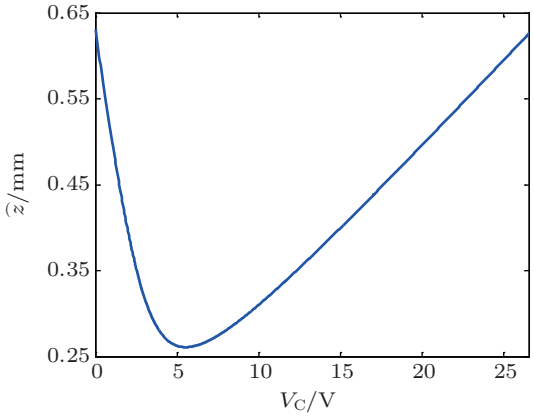


Fig. 11. (color online) Simulated variation of vibration amplitude $\widehat{z}$ with charging voltage $V_C(t)$.

4. Conclusions

Technological advances in power electronics and microfabrication have opened up the possibility of self-powered low-power devices.[43–47] To facilitate the realization of this, current research trends call for harvesting energy from the ambient environment, especially from the ambient mechanical vibration. In most cases, the energy harvested from the mechan-

ical vibration is time-varying and insufficient to power low-power devices directly. Thus a storage device is usually required to accumulate the harvested energy for the intermittent use of low-power devices. In this paper, the transient charging behavior of an energy harvesting system including a PEH, a bridge rectifier, and a storage capacitor is modeled and analyzed under the in-phase assumption. It is found that the charging voltage and the accumulated power increase as the charging process proceeds, but the charging rate decays over time. Moreover, due to the added electrical damping and the change in the system natural frequency when the charging process is initiated, a sudden drop in the vibration amplitude is observed, which in turn affects the charging rate. In addition, the vibration of the piezoelectric cantilever beam begins to strengthen as the charging voltage approaches the peak value of the piezoelectric voltage, which results from the reducing of electrical damping or charging rate. This electromechanical coupling characteristic can also be demonstrated by the vibration amplitude versus the charging voltage.

The output power of the piezoelectric energy harvesting system can be further increased by optimizing the configurations of the piezoelectric cantilever beam. Work on the conversion efficiency and optimization of the piezoelectric energy harvesting system is currently underway, and will be elaborated upon in separate papers.

Acknowledgment

The authors are indebted to Tang Li-Hua of Nanyang Technological University for helpful discussion.

References

[1] Werner-Allen G, Lorincz K, Ruiz M, Marcillo O, Johnson J, Lees J and Welsh M 2006 *IEEE Internet Comput.* **10** 18
[2] Milenković A, Otto C and Jovanov E 2006 *Comput. Commun.* **29** 2521
[3] Wang Z Q, Zhao Y P and Huang Z P 2010 *Int. J. Eng. Sci.* **48** 140
[4] Fan K Q, Jia J Y, Zhu Y M and Zhang X Y 2011 *Chin. Phys. B* **20** 043401
[5] Fan K Q, Wang W D, Zhu Y M and Zhang X Y 2011 *Sci. China: Phys. Mech. Astron.* **54** 1680
[6] Yuse K, Monnier T, Petit L, Lefeuvre E, Richard C and Guyomar D 2008 *J. Intell. Mater. Syst. Struct.* **19** 387
[7] Patricia M, Feng Q and Paul C 2011 *Int. J. Sens. Netw.* **10** 73
[8] Yick J, Mukherjee B and Ghosal D 2008 *Comput. Netw.* **52** 2292
[9] Lin H B, Cao M S, Yuan J, Wang D W, Zhao Q L and Wang F C 2008 *Chin. Phys. B* **17** 4323
[10] Chen Z S and Yang Y M 2011 *Acta Phys. Sin.* **60** 074301 (in Chinese)
[11] Tang L H and Yang Y W 2012 *Appl. Phys. Lett.* **101** 094102
[12] Tang L H, Yang Y W and Soh C K 2012 *J. Intell. Mater. Syst. Struct.* **23** 1433
[13] Sun S and Cao S Q 2012 *Acta Phys. Sin.* **61** 210505 (in Chinese)
[14] Hu Y T, Xue H and Hu H P 2007 *Smart Mater. Struct.* **16** 1961
[15] Stewart M, Weaver P M and Cain M 2012 *Appl. Phys. Lett.* **100** 073901
[16] Xie J M, Yang J S, Hu H P, Hu Y T and Chen X D 2012 *J. Intell. Mater. Syst. Struct.* **23** 135
[17] Shu Y C and Lien I C 2006 *Smart Mater. Struct.* **15** 1499
[18] Renaud M, Karakaya K, Sterken T, Fiorini P, Van Hoof C and Puers R 2008 *Sens. Actuators A* **145** 380
[19] Liang J R and Liao W H 2012 *IEEE. T. Ind. Electron.* **59** 1950
[20] Guan M J and Liao W H 2007 *Smart Mater. Struct.* **16** 498
[21] Lefeuvre E, Badel A, Richard C and Guyomar D 2005 *J. Intell. Mater. Syst. Struct.* **16** 865
[22] Lefeuvre E, Badel A, Benayad A, Lebrun L, Richard C and Guyomar D 2005 *J. Phys. IV* **128** 177
[23] Lefeuvre E, Badel A, Richard C, Petit L and Guyomar D 2006 *Sens. Actuators A* **126** 405
[24] Liu W Q, Feng Z H, He J and Liu R B 2007 *Smart Mater. Struct.* **16** 2130
[25] Hu Y T, Xue H, Hu T and Hu H P 2009 *IEEE T. Ultrason. Ferroelectr. Freq. Control* **55** 148
[26] Ming Z F and Zhou M C 2011 *IEEE. T. Ind. Electron.* **58** 2345
[27] Wu W J, Wickenheiser A M, Reissman T and Garcia E 2009 *Smart Mater. Struct.* **18** 055012
[28] Guan M J and Liao W H 2008 *J. Intell. Mater. Syst. Struct.* **19** 671
[29] Wickenheiser A M, Reissman T, Wu W J and Garcia E 2010 *IEEE ASME T. Mech.* **15** 400
[30] Fang H B, Liu J Q, Xu Z Y, Dong L, Wang L, Chen D, Cai B C and Liu Y 2006 *Microelectr. J.* **37** 1280
[31] Erturk A and Inman D J 2008 *J. Vib. Acoust.* **130** 041002
[32] Erturk A and Inman D J 2008 *J. Intell. Mater. Syst. Struct.* **19** 1311
[33] Benasciutti D, Moro L, Zelenika S and Brusa E 2010 *Microsyst. Technol.* **16** 657
[34] Roundy S and Wright P K 2004 *Smart Mater. Struct.* **13** 1131
[35] Jiang S N, Li X F, Guo S H, Hu Y T, Yang J S and Jiang Q 2005 *Smart Mater. Struct.* **14** 769
[36] Shu Y C and Lien I C 2006 *J. Micromech. Microeng.* **16** 2429
[37] Zhou L, Sun J, Zheng X J, Deng S F, Zhao J H, Peng S T, Zhang Y, Wang X Y and Cheng H B 2012 *Sens. Actuators A* **179** 185
[38] Ajitsaria J, Choe S Y, Shen D and Kim D J 2007 *Smart Mater. Struct.* **16** 447
[39] Ng T H and Liao W H 2005 *J. Intell. Mater. Syst. Struct.* **16** 785
[40] Guyomar D N, Badel A, Lefeuvre E and Richard C 2005 *IEEE T. Ultrason. Ferr.* **52** 584
[41] Ren Q, Zhao Y P, Han L and Zhao H B 2006 *Nanotechnology* **17** 1778
[42] Szarka G D, Stark B H and Burrow S G 2012 *IEEE T. Power Electr.* **27** 803
[43] He C, Chen H, Bai F, Fan Z, Sun L, Xu F, Wang J, Liu Y and Zhu K 2012 *J. Appl. Phys.* **112** 126102
[44] He C, Fu X, Xu F, Wang J, Zhu K, Du C and Liu Y 2012 *Chin. Phys. B* **21** 054207
[45] He C, Chen H, Sun L, Wang J, Xu F, Du C, Zhu K and Liu Y 2012 *Crystal Res. Technol.* **47** 610
[46] He C, Xu F, Wang J, Du C, Zhu K and Liu Y 2011 *J. Appl. Phys.* **110** 083513
[47] He C, Xu F, Wang J and Liu Y 2009 *Crystal Res. Technol.* **44** 211